Global-local analysis of laminated plates by node-dependent kinematic finite elements with variable ESL/LW capabilities

Global-local analysis of laminated plates by node-dependent kinematic finite elements with variable ESL/LW capabilities

E. Zappino, G. Li, A. Pagani, and E. Carrera

MUL^2 Group, Department of Mechanical and Aerospace Engineering, Politecnico di Torino, Corso Duca degli Abruzzi 24, 10129 Torino, Italy.

Keywords:
laminated plates, Carrera Unified Formulation, global-local analysis, node-dependent kinematics.

Author and address for Correspondence
Dr. Enrico Zappino
Department of Mechanical and Aerospace Engineering
Politecnico di Torino,
Corso Duca degli Abruzzi, 24,
10129 Torino, ITALY,
Tel: +39 0110906887, Fax: +39 0110906899
E-mail: enrico.zappino@polito.it

Abstract

This work presents a class of plate finite elements (FEs) formulated with node-dependent kinematics, which can be used to construct global-local models with high numerical efficiency. Taking advantage of Carrera Unified Formulation (CUF), plate theory kinematics can be individually defined on each FE node, realizing a variation of refinement levels within the in-plane domain of one element. When used in the bridging zone between a global model and a locally refined one, an efficient global-local model can be constructed. Elements with variable ESL/LW kinematics from node to node are developed and applied in the global-local analysis of laminated structures. This work includes numerical examples in which LW models with refined kinematics are employed in local regions while ESL models are adopted in the less critical area, and modeling domains are connected by transition zone composed of elements with node-dependent kinematics. The obtained results are compared with solutions from literature and 3D FE modeling. For laminated plates with local effects to be considered, the proposed plate models can reduce the computational costs significantly while guaranteeing numerical accuracy without using special global-local coupling methods.

1 Introduction

Application of composite laminated structures to improve the structural efficiency is drawing increasing attention in many engineering fields especially in aerospace. Sophisticated local effects that cause stress concentration in laminated structures raise the demands for efficient numerical solution approaches.

The simplest 2D model is the well-known Classical Plate Theory (CPT) [1] based on Kirchoff-Love's hypothesis. To take the transverse strains into consideration, First-order Shear Deformation Theory (FSDT) [2] was proposed, which can also been referred to as Reissner-Mindlin model. In the last two decades, a variety of Higher-order Theories (HOT) have also been suggested for the analysis of thin-walled structures. Carrera [3] proposed Unified Formulation (CUF) as a new framework to build refined 2D models. CUF introduces thickness functions $F_\tau(z)$ (employing either series expansion or interpolation polynomials) to formulate the kinematics through the thickness, with which both Equivalent Single Layer (ESL) and Layer-wise (LW) models can be described in a unified manner. Numerical accuracy can be improved by increasing the theory approximation order inherently without the cumbersome derivation of governing equations thanks to the employment of *fundamental nuclei* (FNs), see [4, 5]. Such an advantage leads to a variety of models with variable kinematics, such as those presented by Cinefra et al. [6] and Cinefra and Valvano [7].

In FE analysis, traditionally, to increase the numerical accuracy and capture local stress concentration, the h-version approach [8] is used to increase the mesh refinement while the p-version refinement [9] uses higher order polynomials as shape functions. In contrast, the h-p-version method combines these two approaches [10]. Since in this type of FE models only one set of mesh employing a globally defined kinematic theory exists, and the focus is on the refinement of mesh or element order rather than kinematic theories, they can be distinguished as mono-model approaches.

In multi-model methods, kinematically inconsistent models (e.g., 2D/3D FEs [11, 12], or classical 2D/HOTs, etc.) are combined in a global-local scenario. In a sequential multi-model approach, a subsequent locally refined model is subjected to boundary conditions determined by a global model with less-refined kinematics in a previous step. Due to their intrinsic characteristics, sequential multi-model methods are difficult to be extended to nonlinear cases. This drawback can be overcome by iterative sequential methods, in which the global and local models are solved simultaneously, and an equilibrium needs to be established on their boundaries. Whitcomb and Woo [13, 13] extended this method to geometrically nonlinear problems.

A variety of simultaneous multi-model approaches have been proposed for global-local analysis, in which different FE models are employed separately in different regions, then the compatibility is

enforced at region interfaces or in the overlapping zone. Fish et al. [14] developed an accelerated multi-grid method with an iterative process of information sharing between coarse and fine meshes. Fish [15] presented s-version method to improve the accuracy in the local domain by superimposing additional elements with higher-order kinematics on the global model, in which homogeneous boundary conditions on the superimposed field were used to guarantee the continuity of displacement. Park et al. [16] proposed a similar method which refined the local mesh. The s-version FE method can also be used in combination with h-version and p-version approaches in a simultaneous way, as summarized by Reddy and Robbins [17] and Reddy [18].

Three-field formulations introduce displacements at domain interfaces, then enforce the displacement compatibility with Lagrange multipliers. Prager [19] proposed an interface potential utilizing Lagrange multipliers. Aminpour et al. [20], and Ransom [21] adopted a spline method to couple two domains with different meshes. Adoption of similar approaches was also reported by Brezzi and Marini [22]. Blanco et al. [23, 24] presented an eXtended Variational Formulation (XVF) to couple non-matching kinematic models through two newly introduced Lagrange multiplier fields, which was lately employed by Wenzel et al. [25] in building global-local models. Carrera and Pagani [26, 27, 28] also utilized Lagrange multipliers in refined beam models for global-local analysis.

Two solutions domains can also be connected by an overlapping zone. Dhia [29] and Dhia and Rateau [30] suggested the Arlequin method to enforce compatibility within the overlapping domain with Lagrange multipliers. The Arlequin method has also been implemented in in the framework of CUF by Biscani et al. [31] for beam models and plate models [32, 33]. He et al.[34] adopted Arlequin method to bridge low- and high-order models constructed with CUF, and Constrained Variational Principle (CVP) was used to derive beam elements for multi-layered structures with individual kinematics in each layer.

For multi-layered structures, a simple approach to reduce the computational consumption is grouping the plies into sub-laminates [35, 36] each can be further characterized by independent kinematic theory [37]. Robbins and Reddy [38] proposed variable kinematic finite elements (VKFE) by superposing different types of assumed displacement fields (LW and ESL) within the same element domain, in which homogeneous essential boundary conditions are imposed on the optional and incremental LW variables to the basic ESL ones to maintain the displacement continuity between different types of elements.

CUF provides the convenience to implement node-dependent kinematics by writing theory approximation order as a function of the approximation domain and by making extensive use of index notation, which allows the governing equations in the form of FE arrays to be written in a compact form, see [39]. CUF-based FE models increase the number of degrees of freedom at each node to better approximate the structural responses. For refined plate models, different nodal thickness functions F_τ^i can be integrated with the nodal Lagrangian shape functions N_i to construct advanced elements. Such a methodology permits the connection of domains with different kinematic models by commonly used Lagrangian shape functions, keeping the continuity of displacement field without any *ad hoc* coupling method, and reduces the complexity of the numerical methods greatly. A natural and important application of node-dependent kinematics is building global-local FE models. Carrera and Zappino [40] firstly proposed such an approach, then extended it to the analysis of composite structures with advanced beam models [41]. Plate elements adopting node-dependent kinematics with variable ESL models for multi-layered structures were also proposed by Carrera et al. [42].

In the present article, node-dependent kinematics are applied to construct plate FE models for the global-local analysis of multi-layered structures, and particular attention is paid to the application of elements with variable ESL/LE capabilities used to bridge a locally refined model to a global less-refined one. The FE governing equations for plate models with node-dependent kinematics are derived by applying the Principle of Virtual Displacement (PVD). The assembly of FE stiffness matrix and load vector is elaborated. The proposed approach is assessed with three numerical cases including

both laminated composite plates and sandwich structure. The obtained results are compared against solutions provided by literature or 3D FE modeling.

2 Preliminaries

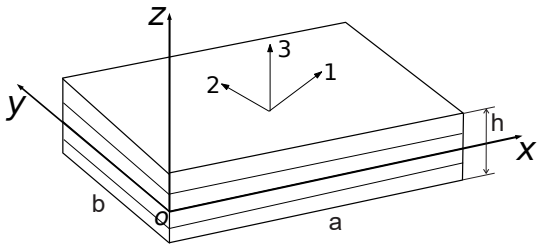

Figure 1: Geometry and reference system of a laminated plate model.

The reference system and the geometry of the multi-layered plate are given in Fig. 1. For displacement-based plate theories, the strain and stress components can be arranged as follows:

$$\boldsymbol{\epsilon}_p^T = \{\epsilon_{xx}, \epsilon_{yy}, \epsilon_{xy}\}, \quad \boldsymbol{\epsilon}_n^T = \{\epsilon_{xz}, \epsilon_{yz}, \epsilon_{zz}\}. \tag{1}$$

$$\boldsymbol{\sigma}_p^T = \{\sigma_{xx}, \sigma_{yy}, \sigma_{xy}\}, \quad \boldsymbol{\sigma}_n^T = \{\sigma_{xz}, \sigma_{yz}, \sigma_{zz}\}. \tag{2}$$

where the subscript p and n indicate the in-plane and out-of-plane components, respectively. The strain vector $\boldsymbol{\epsilon}_p$ and $\boldsymbol{\epsilon}_n$ can be obtained via the geometrical equations:

$$\boldsymbol{\epsilon}_p = \boldsymbol{D}_p \boldsymbol{u}, \qquad \boldsymbol{\epsilon}_n = (\boldsymbol{D}_{np} + \boldsymbol{D}_{nz})\boldsymbol{u}. \tag{3}$$

the explicit expressions of the differential operator matrices are as follows:

$$\boldsymbol{D}_p = \begin{bmatrix} \partial_x & 0 & 0 \\ 0 & \partial_y & 0 \\ \partial_y & \partial_x & 0 \end{bmatrix}, \quad \boldsymbol{D}_{np} = \begin{bmatrix} 0 & 0 & \partial_x \\ 0 & 0 & \partial_y \\ 0 & 0 & 0 \end{bmatrix}, \quad \boldsymbol{D}_{nz} = \begin{bmatrix} \partial_z & 0 & 0 \\ 0 & \partial_z & 0 \\ 0 & 0 & \partial_z \end{bmatrix} \tag{4}$$

The stress components can be attained through the constitutive equations as follows:

$$\boldsymbol{\sigma}_p = \tilde{\boldsymbol{C}}_{pp}\boldsymbol{\epsilon}_p + \tilde{\boldsymbol{C}}_{pn}\boldsymbol{\epsilon}_n, \qquad \boldsymbol{\sigma}_n = \tilde{\boldsymbol{C}}_{np}\boldsymbol{\epsilon}_p + \tilde{\boldsymbol{C}}_{nn}\boldsymbol{\epsilon}_n. \tag{5}$$

where $\tilde{\boldsymbol{C}}_{pp}$, $\tilde{\boldsymbol{C}}_{pn}$, $\tilde{\boldsymbol{C}}_{np}$, and $\tilde{\boldsymbol{C}}_{nn}$ are the matrices of material coefficients defined in the general physical system (x, y, z), whose original forms defined in the material coordinate system (1,2,3) before rotation are as follows:

$$\begin{aligned} \boldsymbol{C}_{pp} &= \begin{bmatrix} C_{11} & C_{12} & C_{16} \\ C_{12} & C_{22} & C_{26} \\ C_{16} & C_{26} & C_{66} \end{bmatrix} & \boldsymbol{C}_{pn} &= \begin{bmatrix} 0 & 0 & C_{13} \\ 0 & 0 & C_{23} \\ 0 & 0 & C_{36} \end{bmatrix} \\ \boldsymbol{C}_{np} &= \begin{bmatrix} 0 & 0 & 0 \\ 0 & 0 & 0 \\ C_{13} & C_{23} & C_{36} \end{bmatrix} & \boldsymbol{C}_{nn} &= \begin{bmatrix} C_{55} & C_{45} & 0 \\ C_{45} & C_{44} & 0 \\ 0 & 0 & C_{33} \end{bmatrix} \end{aligned} \tag{6}$$

in which the material coefficients are determined by the Young's moduli E_1, E_2, E_3, the shear moduli G_{12}, G_{13}, G_{23} and Poisson ratios ν_{12}, ν_{13}, ν_{23}, ν_{21}, ν_{31}, ν_{32}.

3 Carrera Unified Formulation

According to CUF, the displacement field $\boldsymbol{u} = \{u, v, w\}^T$ can be expressed by means of approximation functions $F_\tau(z)$ as follows:

$$\begin{cases} u(x,y,z) = F_0(z)u_0(x,y) & +F_1(z)u_1(x,y) & +\cdots+F_N(z)u_N(x,y) \\ v(x,y,z) = F_0(z)v_0(x,y) & +F_1(z)v_1(x,y) & +\cdots+F_N(z)v_N(x,y) \\ w(x,y,z) = F_0(z)w_0(x,y) & +F_1(z)w_1(x,y) & +\cdots+F_N(z)w_N(x,y) \end{cases} \tag{7}$$

In a more compact form, CUF can be written as shown in Eq. (8) for ESL models and Eq. (9) for LW models, respectively:

$$\boldsymbol{u}(x,y,z) = F_\tau(z)\boldsymbol{u}_\tau(x,y) \qquad \tau = 0,1,...,N \tag{8}$$

$$\boldsymbol{u}^k(x,y,\zeta_k) = F_\tau^k(\zeta_k)\boldsymbol{u}_\tau(x,y); \qquad \tau = 0,1,...,N \tag{9}$$

where k is the layer index in laminated plates. $F_\tau^{(k)}$ are also named as thickness functions in the context of 2D models since they are defined in the thickness domain $z \in [-\frac{h}{2}, \frac{h}{2}]$ for ESL models or $\zeta_k \in [-1, 1]$ for LW models. N is the number of series expansion (except the constant term) adopted in the thickness direction for ESL or the number of interpolation points in layer k for LW models. $\boldsymbol{u}_\tau^{(k)}(x,y)$ represent the unknown primary variables which are the coefficients corresponding to expansion terms $F_\tau^{(k)}$. τ is Einstein's summation subscript. Unlike ESL models, in LW models primary variables are allocated to each layer.

CUF provides a convenient approach in implementing different series expansions and interpolation polynomials in a unified manner to construct refined 2D kinematics for multi-layered structures.

3.1 ESL models adopting Taylor expansions (TE)

CUF can be used to describe many traditional deformation theories. When $F_\tau(z)$ are defined in the whole through-the-thickness domain using ESL model, by substituting $F_\tau = z^\tau (\tau = 0, 1, \cdots, N)$ as shown in Eq. (10), one obtains Higher-order Deformation Theories. As an example, FSDT [2] can be obtained as a degenerated case of the complete linear model with $N = 1$. Since in this class of models Taylor series expansion is used to in the formulation, they can be denoted as TE.

$$F_0 = z^0 = 1, \quad F_1 = z^1 = z, \quad \ldots, \quad F_N = z^N \tag{10}$$

Because of the intrinsic anisotropy of multi-layered structures, the first order derivative of the displacement variables through the thickness might be discontinuous. Fortunately, with ESL models, it is possible to capture the zig-zag effects by employing the Murakami theory [43]. A zig-zag term can be introduced into Equation (8), leading to so-called zig-zag models shown as follows:

$$\boldsymbol{u} = F_0\,\boldsymbol{u}_0 + \ldots + F_N\,\boldsymbol{u}_N + (-1)^k\zeta_k\boldsymbol{u}_Z. \tag{11}$$

in which the subscript Z indicates the introduced zig-zag term. Refined theories can be obtained by adding the zig-zag term to the Taylor polynomials expansion, leading to models denoted as TEnZ.

3.2 LW models based on Lagrange expansions (LE)

Alternatively, if F_τ^k represents Lagrange interpolation polynomials defined in the isoparametric thickness domain of layer k ($\zeta_k \in [-1, 1]$), as shown in Eq. (12), CUF will lead to a LW model based on Lagrange

polynomials. ζ_{k_τ} are located at the prescribed interpolation nodes. $\zeta_{k_0} = -1$ and $\zeta_{k_N} = 1$ correspond to the bottom and top surfaces of the kth layer in the natural reference system, respectively.

$$F_\tau^k(\zeta_k) = \prod_{i=0, i\neq s}^{N} \frac{\zeta_k - \zeta_{k_i}}{\zeta_{k_\tau} - \zeta_{k_i}} \tag{12}$$

In LW models employing Lagrange expansions, the displacements on each interpolation points are used as unknown primary variables, and displacements at layer interfaces obey the following compatibility conditions:

$$u_t^k = u_b^{k+1}, \qquad k = 1, N_l - 1. \tag{13}$$

where N_l represents the total number of layers in the laminated plate. The continuity of transverse stresses at layer interfaces can be satisfied when LW models with a sufficient number of expansion terms are adopted, which has been demonstrated in the authors' previous work [4].

4 Plate elements with node-dependent kinematics

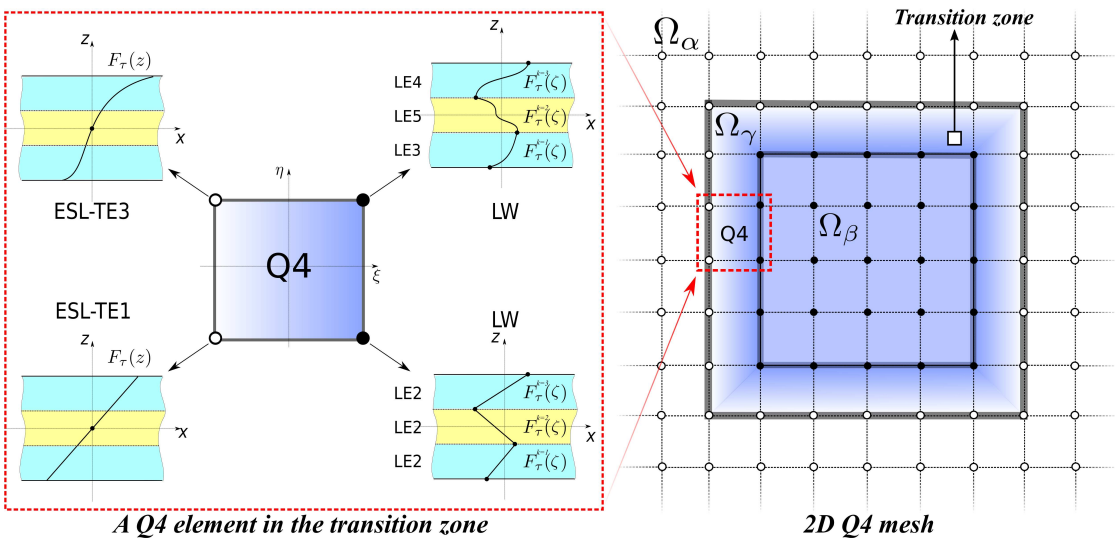

Figure 2: A global-local FE model with node-dependent kinematics.

As discussed in the previous section, CUF introduces thickness functions $F_\tau^{(k)}$ to build refined plate models. At the same time, commonly used plate finite elements employ Lagrangian shape functions to approximate the in-plane displacements. For a plate element with M nodes, the 3D displacement field can be discretized as follows:

$$\boldsymbol{u}^{(k)}(x, y, z) = N_i(x, y) F_\tau^{(k)}(z) \boldsymbol{u}_{i\tau} \qquad \tau = 1, \cdots, N; \quad i = 1, \cdots, M. \tag{14}$$

in which i is the node index, and M represents the number of nodes in a plate element. $\boldsymbol{u}_{i\tau}$ is the vector of nodal primary unknowns. In such an approach, the nodal displacements are firstly approximated by the thickness functions $F_\tau^{(k)}$ through the thickness, then interpolated by the Lagrangian shape functions N_i over the in-plane domain of the plate element. If $F_\tau^{(k)}$ is further related to node i,

then $F_\tau^{i(k)}$ describes thickness kinematics attached to node i; thus CUF-type 2D models can be written as follows:

$$\boldsymbol{u}(x,y,z) = N_i(x,y)F_\tau^{i(k)}(z)\boldsymbol{u}_{i\tau} \qquad \tau = 1,\cdots,N; \quad i = 1,\cdots,M. \tag{15}$$

Eq. (15) implies that the nodal kinematics $F_\tau^{i(k)}$ are further integrated by the nodal Lagrangian shape functions N_i to construct a finite element. The thickness functions attached to each node can be assumed according to any applicable theory, either ESL or LW.

Fig. 2 illustrates a Q4 element as an example, in which on each of the four nodes distinct thickness kinematics are adopted (namely TE1, TE3, LE2, and LE3/LE5/LE4). Such an element can realize a "kinematic variation", bridging a less-refined model to a locally refined one, leading to a global-local FE model. Distinguished from the coupling methods discussed in the introduction section, in this approach a transition zone is introduced. Within the transition zone, the elements employ variable node-dependent kinematics from node to node, which means that the kinematic description of each node is individually defined and a natural kinematic transition can be realized over the domain of an element. Higher-order theories can be used on the side connected to the local model, while lower-order models on the other side close to the peripheral region.

For this type of global-local FE models with node-dependent kinematics, a kinematic variation can be achieved with the commonly used Lagrangian shape functions, which avoids any *ad hoc* assumption and leads to advanced models with compact FE formulations. Such a bridging method can naturally result in continuous displacement field. This approach can be used in combination with h-version, p-version or $h-p$-version mesh refinement to increase numerical accuracy.

4.1 FE governing equations

The governing equations for plate elements with node-dependent kinematics are derived by applying the Principle of Virtual Displacements (PVD). For a static problem, one has:

$$\delta L_{int} = \delta L_{ext} \tag{16}$$

where L_{int} represents the strain energy due to the external load, and L_{ext} stands for the work done by the external load on the virtual displacements. δ indicates the virtual variation. The internal work can be expressed as:

$$\delta L_{int} = \int_V \delta\boldsymbol{\epsilon}^T\boldsymbol{\sigma}dV = \int_\Omega\int_{A_k}\delta\boldsymbol{\epsilon}^T\boldsymbol{\sigma}dA_k d\Omega \tag{17}$$

in which Ω represents the in-plane domain of an element el, and A_k indicates the through-the-thickness domain corresponding to layer k. Eq. (17) elucidates that the unit integration domain is restrict within a domain determined by layer k and element el. Utilizing CUF, the displacement field in the domain confined within element el and layer k can be expressed as shown in Eq. (18) for ESL models, in which $z \in [z_{bottom}, z_{top}]$:

$$\begin{aligned} \boldsymbol{u}(x,y,z) &= N_i(x,y)F_\tau^i(z)\boldsymbol{u}_{i\tau} \qquad \tau = 1,\cdots,N; \quad i = 1,\cdots,M. \\ \delta\boldsymbol{u}(x,y,z) &= N_j(x,y)F_s^j(z)\delta\boldsymbol{u}_{js} \qquad s = 1,\cdots,N; \quad j = 1,\cdots,M. \end{aligned} \tag{18}$$

Or alternatively in Eq. (19) for LW models, where $\zeta_k \in [-1,1]$:

$$\begin{aligned} \boldsymbol{u}^k(x,y,\zeta_k) &= N_i(x,y)F_\tau^{ik}(\zeta_k)\boldsymbol{u}_{i\tau}^k \qquad \tau = 1,\cdots,N; \quad i = 1,\cdots,M. \\ \delta\boldsymbol{u}^k(x,y,\zeta_k) &= N_j(x,y)F_s^{jk}(\zeta_k)\delta\boldsymbol{u}_{js}^k \qquad s = 1,\cdots,N; \quad j = 1,\cdots,M. \end{aligned} \tag{19}$$

In a compact form, the strain vectors can be obtained as follows in Eq. (20), which is adaptable to both ESL and LW models:

$$\begin{aligned}\boldsymbol{\epsilon}_p^k &= F_\tau^{i(k)} \boldsymbol{D}_p (N_i \boldsymbol{I}) \boldsymbol{u}_{i\tau}^{(k)} \\ \boldsymbol{\epsilon}_n^k &= F_\tau^{i(k)} \boldsymbol{D}_{np} (N_i \boldsymbol{I}) \boldsymbol{u}_{i\tau}^{(k)} + F_{\tau,z}^{i(k)} N_i \boldsymbol{I} \boldsymbol{u}_{i\tau}^{(k)}\end{aligned} \tag{20}$$

where $\boldsymbol{I}$ is a 3×3 identity matrix. Considering the strain expression Eq. (3), the constitutive equations Eq. (5), as well as CUF-type FE displacement expression Eq. (18) or Eq. (19), by applying the principle of virtual displacement, one can obtain the expression of internal work as:

$$\delta L_{int} = \int_\Omega \int_{A_k} (\delta \boldsymbol{\epsilon}_n^{k^T} \boldsymbol{\sigma}_n^k + \delta \boldsymbol{\epsilon}_p^{k^T} \boldsymbol{\sigma}_p^k) dA_k d\Omega = \delta \boldsymbol{u}_{js}^{(k)^T} \boldsymbol{K}_{ij\tau s}^k \boldsymbol{u}_{i\tau}^{(k)} \tag{21}$$

in which the 3×3 matrix $\boldsymbol{K}_{ij\tau s}^k$ is the so-called *fundamental nucleus* (FN) of stiffness in the context of CUF, which is the core unit of the element stiffness matrix. By adopting the Einstein summation convention, the stiffness matrix of the spatial domain identified by Ω and A_k can be obtained.

A generic surface load acting on a horizontal surface of the plate can be denoted as $p_\alpha(x, y)$, where the subscript α indicates the loading direction, which can equal x, y or z. The virtual variation of the external work caused by p_α can be written as Eq. (22):

$$\delta L_{ext}^{p_\alpha} = \int_\Omega \delta u_\alpha^{(k)} p_\alpha d\Omega = \int_\Omega \delta u_{\alpha_{js}}^{(k)} N_j F_s^{j(k)}(z_p) p_\alpha d\Omega \tag{22}$$

in which z_p represents the coordinate of the loading surface. If the external surface load is written into a vector as $\boldsymbol{p}_\alpha(x, y)$ ($\{p_x, 0, 0\}^T$, $\{0, p_y, 0\}^T$, or $\{0, 0, p_z\}^T$), Eq. (22) can be further expressed in a vector form as in Eq. (23), where $\boldsymbol{P}_{js}^{(k)}$ is the FN of external load, in which only the components on α direction are non-zero.

$$\delta L_{ext}^{p_\alpha} = \delta \boldsymbol{u}_{js}^{(k)^T} \boldsymbol{P}_{js}^{(k)} \tag{23}$$

Thus the governing equation can be expressed as follows:

$$\delta \boldsymbol{u}_{js}^{(k)^T} : \quad \boldsymbol{K}_{ij\tau s}^k \boldsymbol{u}_{i\tau}^{(k)} = \boldsymbol{P}_{js}^{(k)} \tag{24}$$

The explicit expressions of the FNs have been given in [42]. For more details about the derivation, the reader is referred to [7] and [39].

4.2 Assembly of the stiffness matrix and load vector

As already declared, a fundamental nucleus is a core unit of the stiffness matrix. By looping on the subscripts of expansions and node indexes, the stiffness matrix on node level can be attained, then be further assembled on the element and structure scale. Such an assembly routine for CUF-based FE models has been elaborated in [39].

When various node-dependent kinematic models are used on different nodes of an element, usually a general sub-matrix K_{ij} would be rectangular rather than square. As an example, Fig. 3 presents the stiffness and load vector assembly of a node-dependent kinematic Q4 plate element *el* with variable ESL/LW capabilities, in which on node a and b LW models are employed, while on node c and d ESL models are adopted. The following cases of the sub-matrices are considered:

- Case 1: $\boldsymbol{K}_{aa}$ and $\boldsymbol{K}_{bb}$: diagonal matrices for LW models with different number of expansions from layer to layer, which are achieved by assembling the stiffness matrices corresponding to each layer and overlapping the components at layer interfaces.

- Case 2: $\boldsymbol{K}_{cc}$ and $\boldsymbol{K}_{dd}$: diagonal matrices for ESL models, in which the stiffness components from different layers are lumped together.

- Case 3: $\boldsymbol{K}_{ab}$ and $\boldsymbol{K}_{ba}$: coupling matrices between LW models; since in PVD the integration to obtain the stiffness matrix is operated on a brick domain defined by element el and layer k, $\boldsymbol{K}_{ab}^{k}$ and $\boldsymbol{K}_{ba}^{k}$ (where k is the layer index) will become rectangular, and after overlapping components at layer interfaces, the location of their components become as shown in Fig. 3, see $\boldsymbol{K}_{ab}^{1}$, $\boldsymbol{K}_{ab}^{2}$, and $\boldsymbol{K}_{ab}^{3}$.

- Case 4: $\boldsymbol{K}_{bd}$ and $\boldsymbol{K}_{db}$: coupling matrices between ESL models with different number of expansions through the thickness.

- Case 5: $\boldsymbol{K}_{ac}$, $\boldsymbol{K}_{ca}$, $\boldsymbol{K}_{bc}$, $\boldsymbol{K}_{cb}$, $\boldsymbol{K}_{ad}$, $\boldsymbol{K}_{da}$, $\boldsymbol{K}_{bd}$, and $\boldsymbol{K}_{db}$: coupling matrices between LW and ESL models; since the stiffness components for ESL models are smeared on each node without distinguishing different layers, the coupling matrices between LW and ESL show banded distribution as illustrated in Fig. 3.

Meanwhile, the shape of the load vector should be assembled in a similar manner, and become compatible with the stiffness matrix, as has been demonstrated in the right-hand-side of Fig. 3. Such an assembly routine is a further development of classical assembly technique for CUF-based FE models.

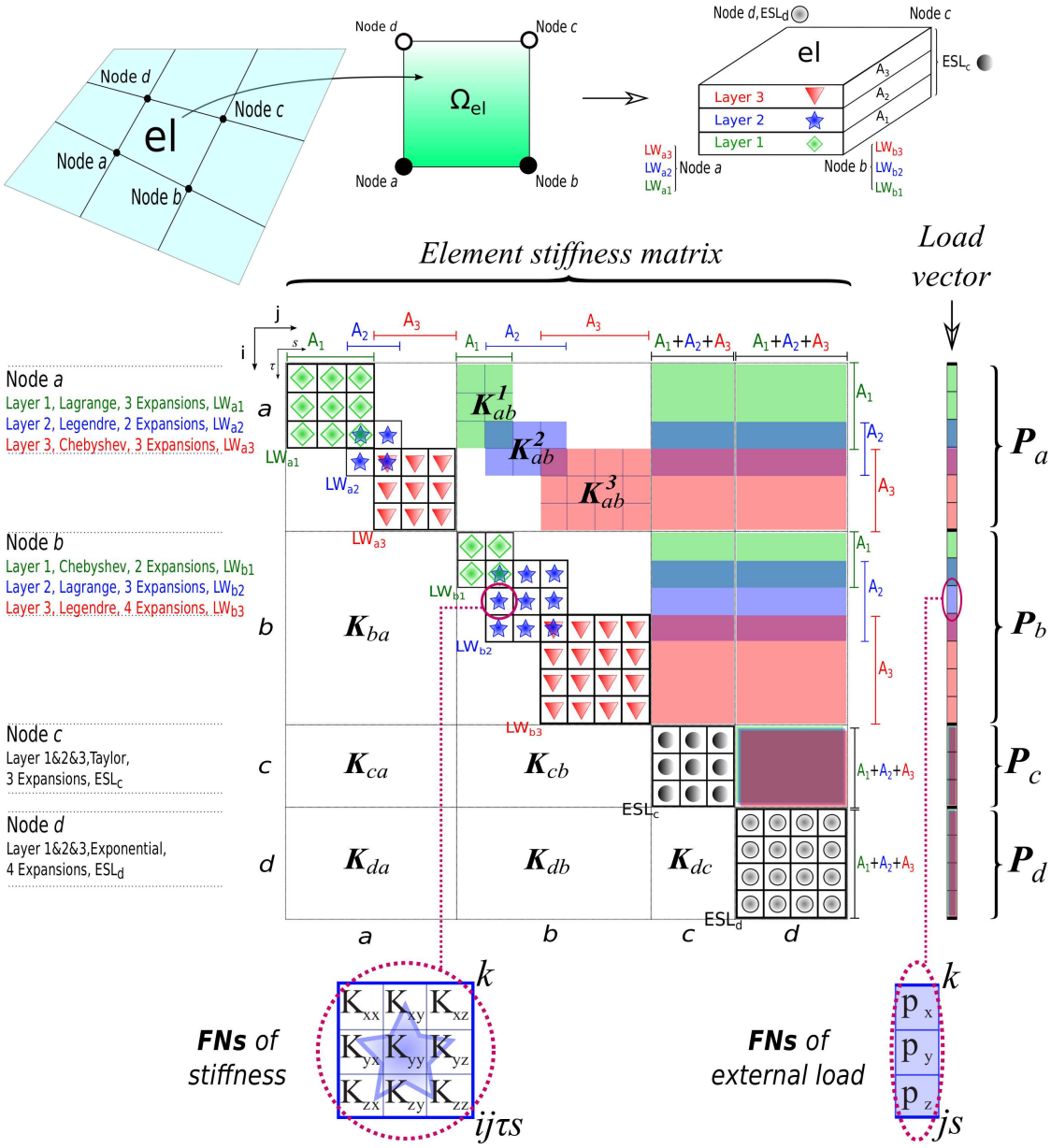

Figure 3: Assembly of the stiffness matrix and load vector on element level.

5 Numerical results

In this section, results on laminated structures obtained with node-dependent kinematic plate models are presented. Corresponding global-local models with variable ESL/LW kinematics are denoted by TEnZ-LEm, in which TEnZ refers to the less-refined kinematic models based on Taylor series used in the region of less interest, and LEm stands for the refined models with Lagrange polynomials employed in the local zone. The transition zone is as wide as the size of one element. Since FSDT give a linear through-the-thickness variation for transverse shear stresses on plates, it is not employed in this article. A MITC9 plate element formulated by Cinefra et al. [44, 6] is adopted in the numerical analysis.

5.1 Eight-layered cantilever composite beam

An eight-layered laminated cantilever beam is considered as the first numerical example. Its geometry feature and stacking sequence are shown in Fig. 4. The beam is loaded to a concentrated load $P = 0.2$N at the central point on the free end and clamped on the other end. The material properties are listed Table 1, in which the subscripts L and T indicate the fiber longitudinal and transverse direction, respectively. Numerical solutions for such a structure has been reported by various authors [45, 46, 47, 48, 41]. In this article the displacement w is reported on point A$(0, b, 0)$, stress σ_{yy} on point B$(0, \frac{b}{2}, \frac{h}{2})$, and σ_{yz} on C$(0, \frac{b}{2}, 0)$. The construction of the global-local FE model is as illustrated in Fig. 4, in which refined kinematics is used on the nodes lie in the central zone along the longitudinal axis of the structure within where the stress σ_{yy} and σ_{yz} are evaluated. The transition zone is as wide as the size of one element, connecting the inner region with LW model to the outer parts with ESL kinematics. Based on the numerical study, mesh grid 2×10 and LW model LE5 can guarantee the convergence, and the corresponding results are in good agreement with solutions from literature.

By observing the results summarized in Table 2, it can be found that compared with LW models, ESL models adopting Taylor series also give reasonable approximations in this case. Compared with the globally defined LE5 model, ESL model TE3Z gives less accurate through-the-thickness variation for σ_{yy} and σ_{yz} on the mid-span cross-section as shown in Fig. 5. While global-local model TE3Z-LE5 leads to results in high agreement with the complete LE5 model at a reduction of 64.6% in degrees of freedom. This example also shows that with node-dependent kinematics, it is convenient to construct a global-local FE model by simply changing the kinematic theories on the desired nodes without any additional operation on the mesh grids.

Table 1: Material properties for the eight-layered cantilever beam.

Material	E_L[GPa]	E_T[GPa]	ν_{LT}	G_{LT}[GPa]
1	30	1	0.25	0.5
2	5	1	0.25	0.5

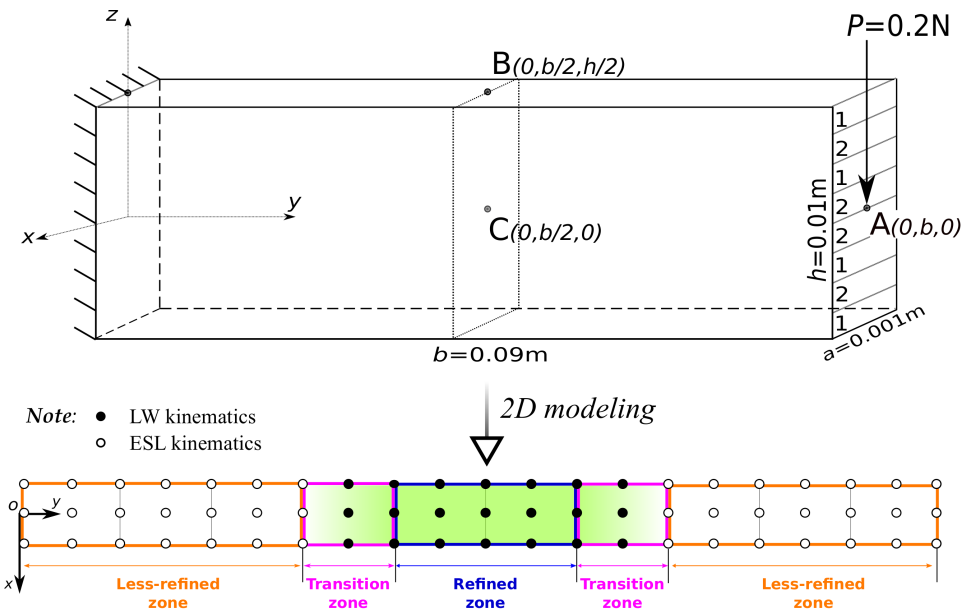

Figure 4: Geometry and FE discretization of the eight-layered cantilever beam.

Table 2: Displacement and stress evaluation obtained with various models for the eight-layered cantilever beam.

Mesh	Kinematics	$w^{\S}$	$\sigma_{yy}^{\dagger}$	$\sigma_{yz}^{\ddagger}$	DOFs	DOF Reduction
		[10^{-2}mm]	[KPa]	[KPa]		
1×5	LE4	-3.034	732.1	-27.87	2475	–
2×10	LE4	-3.033	729.3	-27.77	7875	–
2×10	LE5	-3.033	727.8	-27.41	10395	Reference
2×10	TE1Z	-2.981	729.4	-20.00	945	–
2×10	TE3Z	-3.027	730.0	-28.21	1575	–
2×10	TE5Z	-3.029	730.1	-27.51	2205	–
2×10	TE7Z	-3.029	729.9	-28.62	2835	–
2×10	TE1Z-LE5	-2.991	735.9	-25.72	3195	69.3%
2×10	TE3Z-LE5	-3.028	732.5	-27.94	3675	64.6%
2×10	TE5Z-LE5	-3.029	732.2	-27.79	4155	60.0%
Surana & Nguyen [45]		-3.03	720	–	–	–
Lin & Zhang [46]		-3.03	750	–	–	–
Davalos et al. [47]		-3.06	700	–	–	–
Carrera et al. [41]		-3.05	730	-27.9	4743	–

Variables are evaluated at: §A$(0, b, 0)$; †B$(0, \frac{b}{2}, \frac{h}{2})$; ‡C$(0, \frac{b}{2}, 0)$.

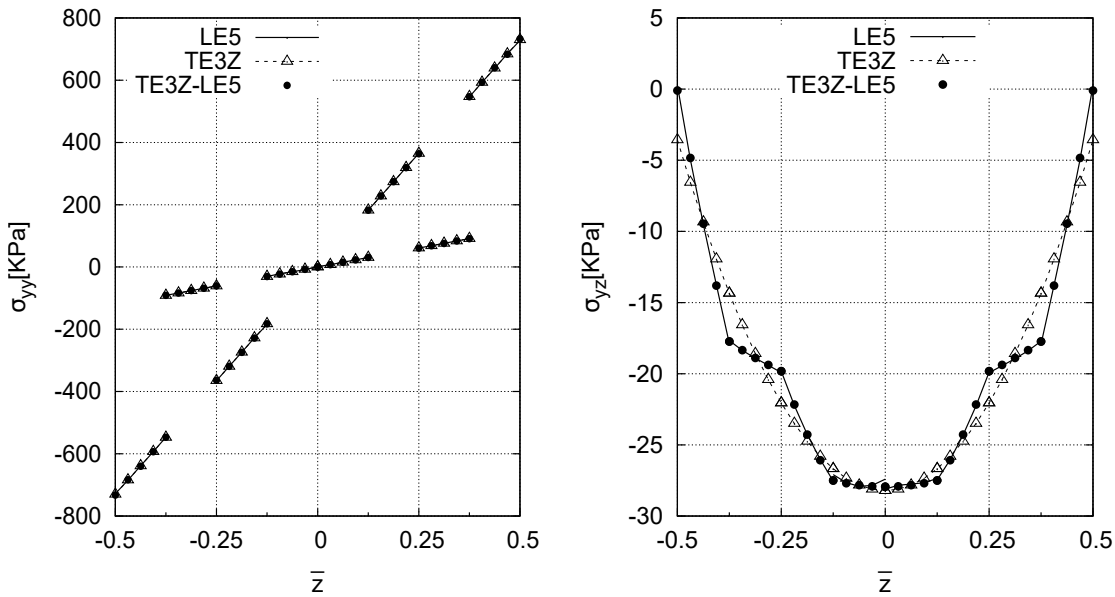

(a) σ_{yy}, $(0, \frac{b}{2}, \bar{z})$ (b) σ_{yz}, $(0, \frac{b}{2}, \bar{z})$

Figure 5: Through-the-thickness variation of stresses on the eight-layered cantilever beam.

5.2 Sandwich plate under simple supports on two parallel edges

The sandwich plate considered is composed of a soft core and two composite faces, with length $a =$ 10mm, width $b =$ 1mm, and height $h =$ 1mm. The sandwich structure is simply supported on two parallel edges $(x = 0, a)$, and loaded to constant pressure $p_0 =$ 1MPa on 10% of the length located at

the central top surface, as shown in Fig. 6(a). The thicknesses of the layers are $0.1h/0.8h/0.1h$. The material properties used are listed in Table 3. Numerical results for this case have also been reported by Wenzel et al. [25] but on different output points.

The global-local FE model with node-dependent kinematics is as shown in Fig. 6(b). Taking advantage of the symmetry feature, 1/4 of the structure is modeled with finite elements, and LW kinematics is used in the region within and near the loading area, connected to the part adopting ESL models by a narrow transition zone composed of elements with variable ESL/LW kinematics from node to node. The results summarized in Table 4 show that CUF-based FE model with mesh grid 40×8 and LW kinematics LE5 can ensure the numerical convergence, and achieve results agree well with those obtained with an ABAQUS 3D model (employing brick element C3D20R).

In sandwich structures, the difference in stiffness usually leads to insignificant stresses in the soft core compared with those in the rigid faces. At the same time, to obtain a linear variation of σ_{zz} through the thickness with a LW model, at least three interpolation points should be used (LE3). To further reduce the computational costs, in the present numerical case, a layer-wisely defined model LE5/LE3/LE5 as shown in Fig. 7 is employed, which can be denoted as LE5/LE3 for brevity. Compared with the complete LE5 model, LE5/LE3 can reduce the degrees of freedom by 15.4% without losing solution accuracy, as listed in Table 4. It can also be found that the global-local models TE3Z-LE5/LE3 and TE5Z-LE5/LE3 give good evaluations on displacement w and the stresses with much fewer computation costs in comparison with the LE5 model.

Fig. 8 compares the through-the-thickness variation of displacement w and stresses attained with different FE models. It can be observed that complete ESL model TE3Z fails to give a reasonable approximation. A complete LE3 model can capture the variation well except on σ_{xz}. Meanwhile, LE5/LE3 and TE3Z-LE5/LE3 lead to results in high agreement with the complete LE5 model. Fig. 9 and Fig. 10 show the comparison on contour plot of σ_{xz} and σ_{zz} between complete LE5 model and global-local model TE3Z-LE5/LE3, respectively. In the local region near the loading area, the stress distribution agrees well with each other; across the transition zone stress oscillation can be observed, yet in the less-critical zone ESL model TE3Z leads to erroneous distribution. The numerical results show that the global-local model TE3Z-LE5/LE3 can give accurate results compared with the complete LE5 model with a reduction of 54.7% in degrees of freedom.

Table 3: Material properties used on the sandwich plate.

	E_{11}[GPa]	E_{22}[GPa]	E_{33}[GPa]	ν_{12}	ν_{13}	ν_{23}	G_{12}[GPa]	G_{13}[GPa]	G_{23}[GPa]
Face	131.1	6.9	6.9	0.32	0.32	0.49	3.588	3.088	2.3322
Core	0.2208×10^{-3}	0.2001×10^{-3}	2.76	0.99	0.00003	0.00003	16.56×10^{-3}	0.5451	0.4554

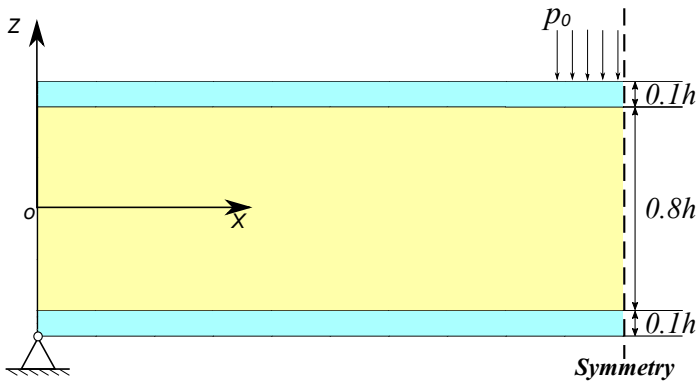

(a) Boundary conditions

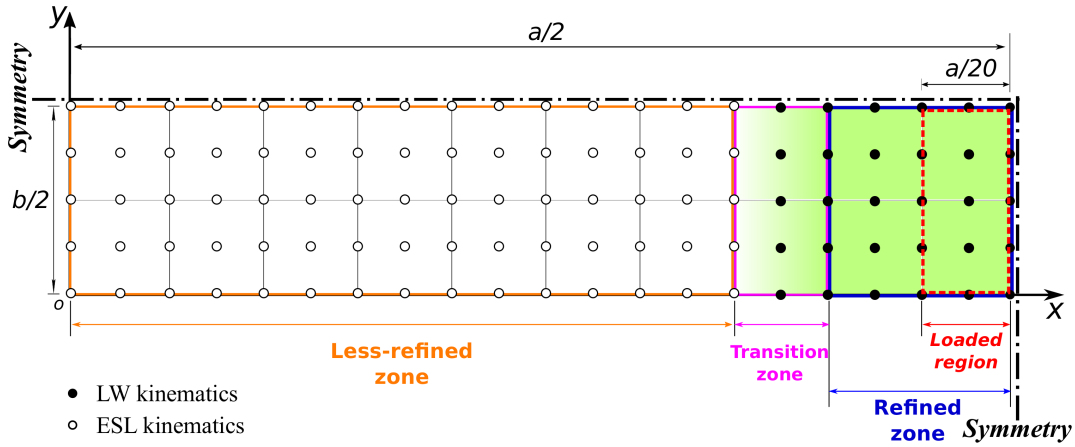

(b) 1/4 FE model with symmetry

Figure 6: Global-local FE model with node-dependent kinematics for the sandwich plate.

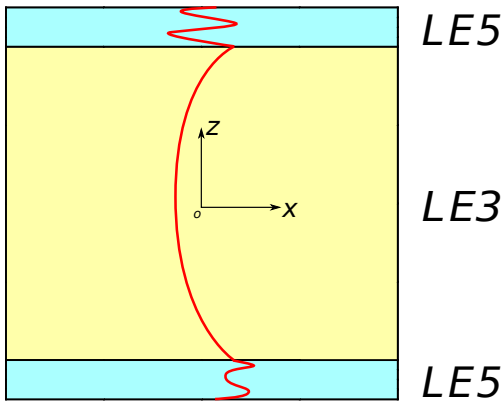

Figure 7: LE5/LE3: through-the-thickness variation of kinematics in the FE model for the sandwich structure.

Table 4: Displacement and stress evaluation obtained with various models for the sandwich plate.

Mesh	Kinematics	$-w^{\S}$	$-\sigma_{xx}^{\dagger}$	$-\sigma_{xz}^{\ddagger}$	$-\sigma_{zz}^{\dagger}$	DOFs	DOF Reduction
		[10^{-3}mm]	[MPa]	[MPa]	[MPa]		
10×2	LE4	2.470	19.22	1.081	0.9036	3150	–
20×4	LE4	2.471	18.26	1.157	1.026	11070	–
40×8	LE4	2.471	18.15	1.177	1.050	41310	–
40×8	LE5	2.471	18.11	1.180	0.9989	53703	Reference
40×8	TE1Z	2.459	13.99	1.626	1.214	12393	–
40×8	TE3Z	2.455	17.82	1.384	2.213	20655	–
40×8	TE5Z	2.468	17.77	1.286	1.587	28917	–
40×8	LE3	2.469	17.60	0.8921	1.023	28917	–
40×8	LE5/LE3(Fig. 7)	2.470	18.09	1.167	0.9989	45441	15.4%
40×8	TE1Z-LE5/LE3	2.472	17.50	1.315	1.000	17289	67.8%
40×8	TE3Z-LE5/LE3	2.463	18.22	1.158	0.9992	24327	54.7%
40×8	TE5Z-LE5/LE3	2.469	18.17	1.156	0.9989	31365	41.6%
ABAQUS-3D		2.471	18.15	1.107	1.001	620787	–

Variables are evaluated at: $^{\S}(\frac{a}{2}, \frac{b}{2}, -\frac{h}{2})$; $^{\dagger}(\frac{a}{2}, \frac{b}{2}, \frac{h}{2})$; $^{\ddagger}(\frac{9a}{20}, 0, \frac{9h}{20})$.

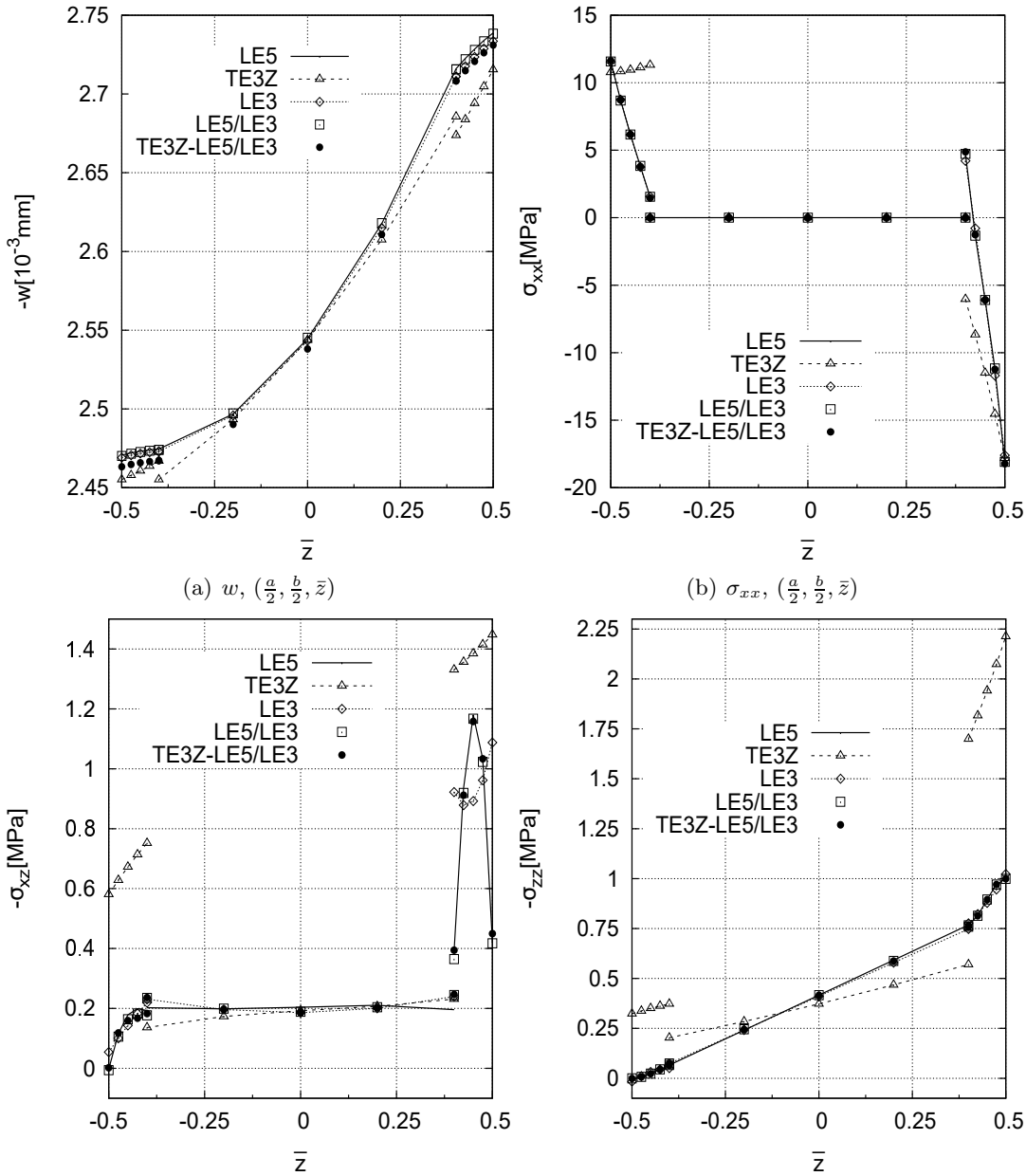

(a) w, $(\frac{a}{2}, \frac{b}{2}, \bar{z})$

(b) σ_{xx}, $(\frac{a}{2}, \frac{b}{2}, \bar{z})$

(c) σ_{xz}, $(\frac{9a}{20}, 0, \bar{z})$

(d) σ_{zz}, $(\frac{a}{2}, \frac{b}{2}, \bar{z})$

Figure 8: Through-the-thickness variation of displacement and stresses on the sandwich plate.

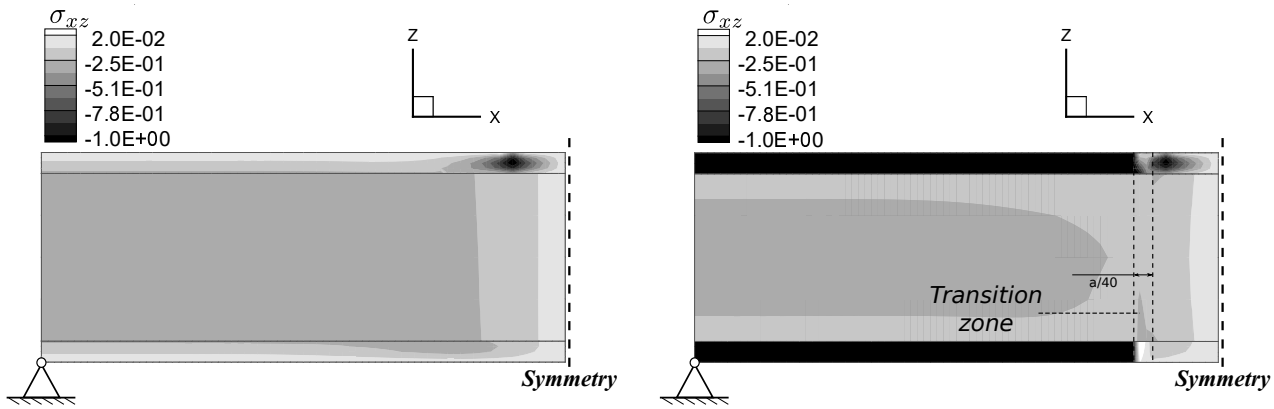

(a) LE5 (b) TE3Z-LE5/LE3

Figure 9: Contour plot of σ_{xz} on the outer surface section ($y = -\frac{b}{2}$) of the sandwich plate.

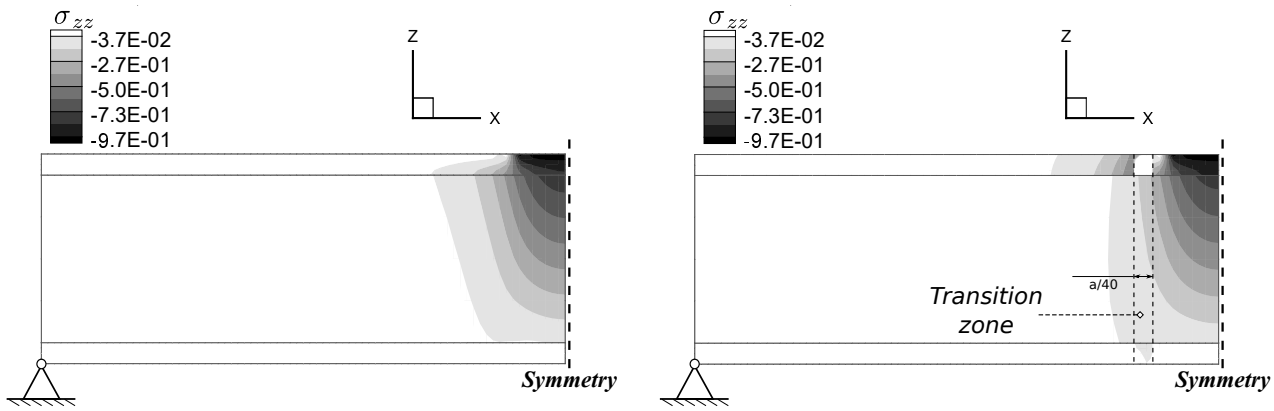

(a) LE5 (b) TE3Z-LE5/LE3

Figure 10: Contour plot of σ_{zz} on the middle surface section ($y = 0$) of the sandwich plate.

5.3 Three-layered composite plate under local pressure load

A there-layered composite plate with stacking sequence [0°/90°/0°] under simply-supported boundary conditions is studied in this section. The length a and width b of the plate are $a = b = 0.1m$. The length to thickness ratio is $a/h = 10$, and the three layers are of equal thickness ($h/3$). The plate undergoes a local uniform transverse pressure load $p_0 = 1$MPa on its top surface within a rectangular region centered at $(a/2, b/2, h/2)$ with side length of $a/5$ and $b/5$. The properties of the material are listed in Table 5, in which L indicates the fiber longitudinal and T the transverse direction. The FE model adopted is as demonstrated in Fig. 11, in which a transition zone consist of elements with node-dependent kinematic variable ESL/LW theories connects a local model employing LW model to a less-refined global model with ESL kinematics. 1/4 of the plate in modeled in combination with symmetry boundary conditions. The reference solutions are provided by Biscani et al. [32].

The result summary in Table 6 show that mesh grid 15×15 employing LE5 can guarantee the numerical convergence. ESL models TE1 and TE1Z fail to give accurate evaluations on the stresses; when LW kinematics LE5 are used on the selected nodes lie in the local model (leading to global-local model TE1-LE5 and TE1Z-LE5, respectively), the numerical accuracy is improved to a great extent. Global-local model TE3Z-LE5 can give good approximations on both displacement w and stresses, as

listed in Table 6. Compared with the FE model with globally defined LE5 kinematics, TE3Z-LE5 reduced the degrees of freedom by 55.1% with comparable accuracy.

By observing the displacement and stress variation shown in Fig. 12, it can be found that TE3Z is not able to capture the accurate distribution of transverse shear stresses, while with the help of the locally defined LE5 kinematics, TE3Z-LE5 model can lead to satisfactory results. The contour plot of σ_{yz} shown in Fig. 13 and σ_{zz} in Fig. 14 compares the complete LE5 model and global-local model TE3Z-LE5, which show that the difference mainly lies in the region outside of the locally refined zone. The results demonstrated that the proposed global-local approach based on node-dependent kinematics is reliable in capturing detailed mechanical responses in local areas of interest.

Table 5: Material properties of the three-layered composite plate.

E_L[GPa]	E_T[GPa]	ν_{LT}	ν_{TT}	G_{LT}[GPa]	G_{TT}[GPa]
132.5	10.8	0.24	0.49	5.7	3.4

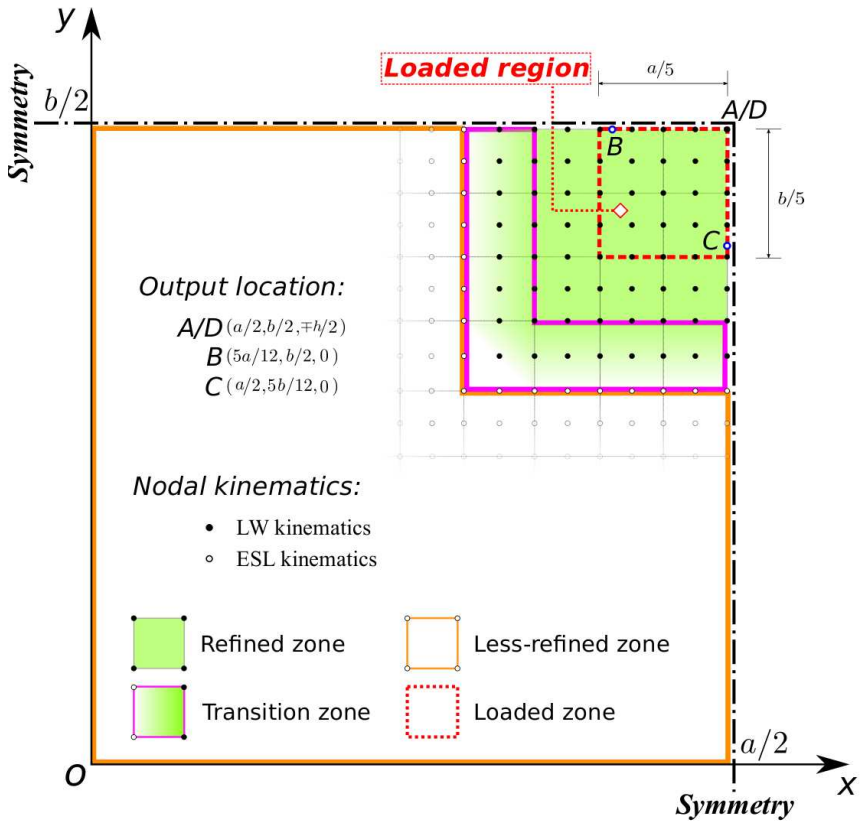

Figure 11: Global-local model with node-dependent kinematics for the three-layered composite plate.

Table 6: Displacement and stress evaluation on the three-layered plate under local pressure, obtained with various models.

Mesh	Kinematics	$-w^{\S}$	$\sigma_{xx}^{\S}$	$\sigma_{yy}^{\S}$	$-10\sigma_{xz}^{\dagger}$	$-10\sigma_{yz}^{\ddagger}$	$-\sigma_{zz}^{\star}$	DOFs	DOF Reduction
		[10^{-5}m]	[MPa]	[MPa]	[MPa]	[MPa]	[MPa]		
5×5	LE4	1.596	1.928	-0.03834	4.662	4.935	0.5375	3630	–
10×10	LE4	1.674	12.07	2.060	6.442	6.874	0.9634	13230	–
15×15	LE4	1.675	12.00	2.041	6.464	6.902	1.006	28830	–
15×15	LE5	1.675	11.99	2.033	6.463	6.902	0.9928	37479	Reference
15×15	TE1	1.591	10.53	1.644	3.829	4.653	1.988	5766	–
15×15	TE1Z	1.577	11.41	2.318	4.667	4.995	1.953	8649	–
15×15	TE3Z	1.672	12.00	2.134	5.647	6.914	1.244	14415	–
15×15	TE1-LE5	1.665	12.19	1.362	6.140	6.886	0.9939	9066	75.8%
15×15	TE1Z-LE5	1.734	12.20	1.394	6.626	7.064	0.9939	11649	68.9%
15×15	TE3Z-LE5	1.674	12.00	2.033	6.471	6.873	0.9928	16815	55.1%
3D–Biscani et al.[32]		1.674	11.94	2.019	6.524	–	–	–	–

Variables are evaluated at: $^{\S}\mathrm{A}(\frac{a}{2}, \frac{b}{2}, -\frac{h}{2})$; $^{\dagger}\mathrm{B}(\frac{5a}{12}, \frac{b}{2}, 0)$; $^{\ddagger}\mathrm{C}(\frac{a}{2}, \frac{5b}{12}, 0)$; $^{\star}\mathrm{D}(\frac{a}{2}, \frac{b}{2}, \frac{h}{2})$.

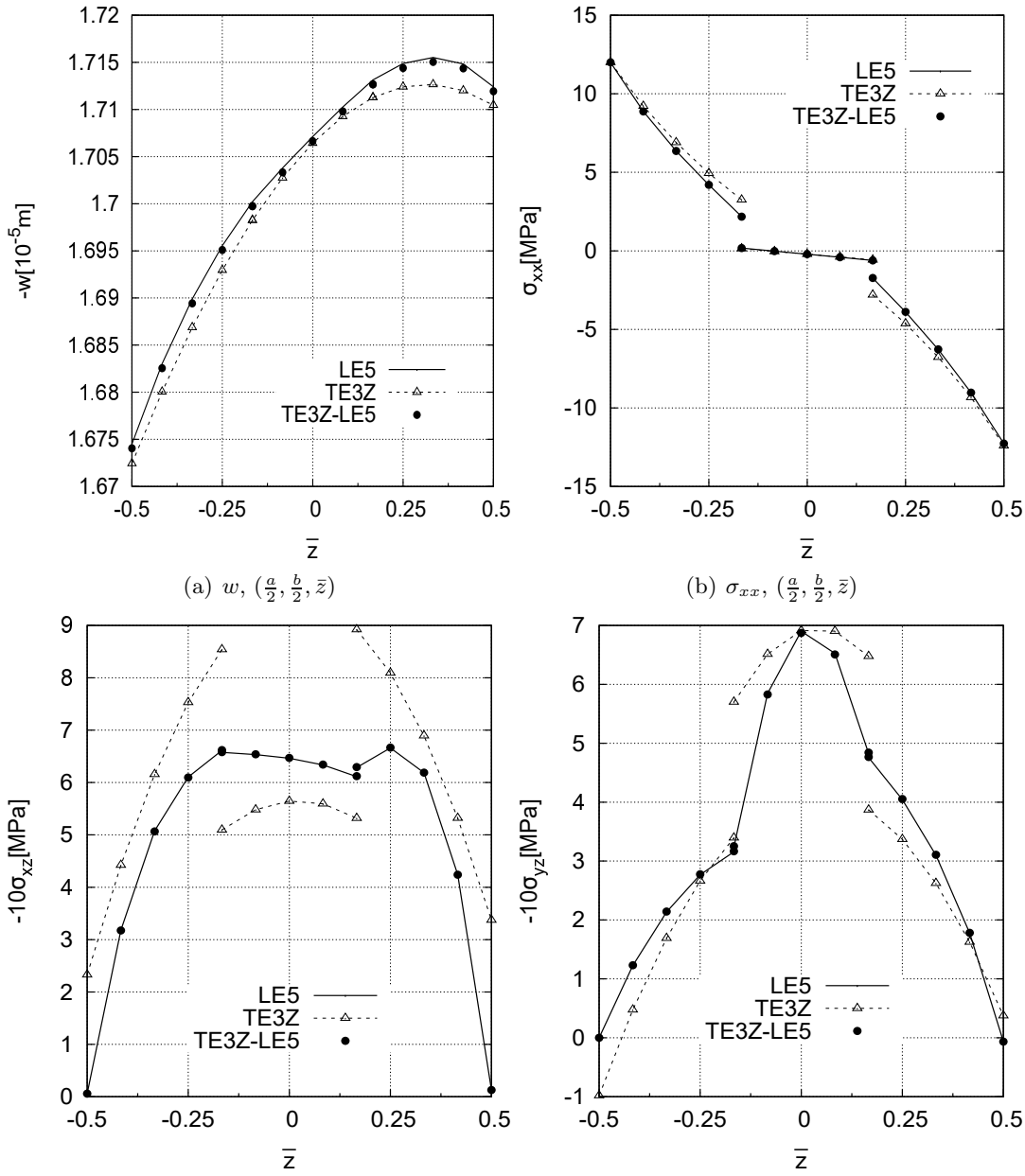

(a) w, $(\frac{a}{2}, \frac{b}{2}, \bar{z})$

(b) σ_{xx}, $(\frac{a}{2}, \frac{b}{2}, \bar{z})$

(c) σ_{xz}, $(\frac{5a}{12}, \frac{b}{2}, \bar{z})$

(d) σ_{yz}, $(\frac{a}{2}, \frac{5b}{12}, \bar{z})$

Figure 12: Through-the-thickness variation of displacement and stresses on the three-layered composite plate under local pressure.

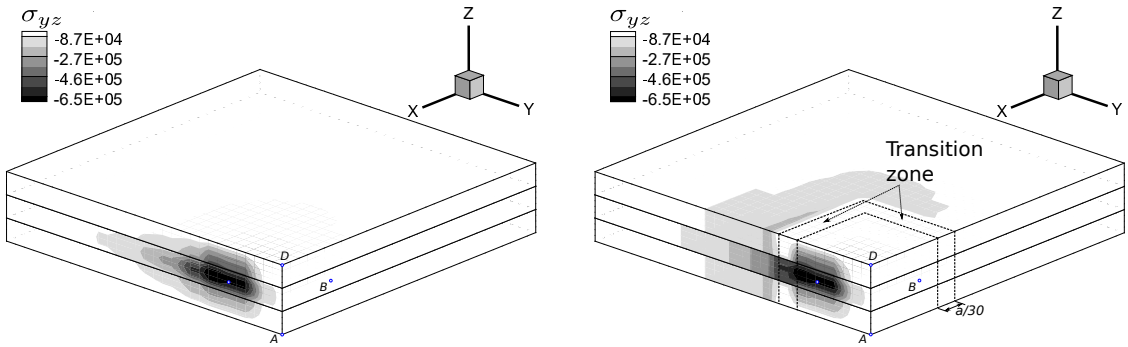

(a) LE5 (b) TE3Z-LE5

Figure 13: Contour plot of σ_{yz} on the three-layered plate under local pressure.

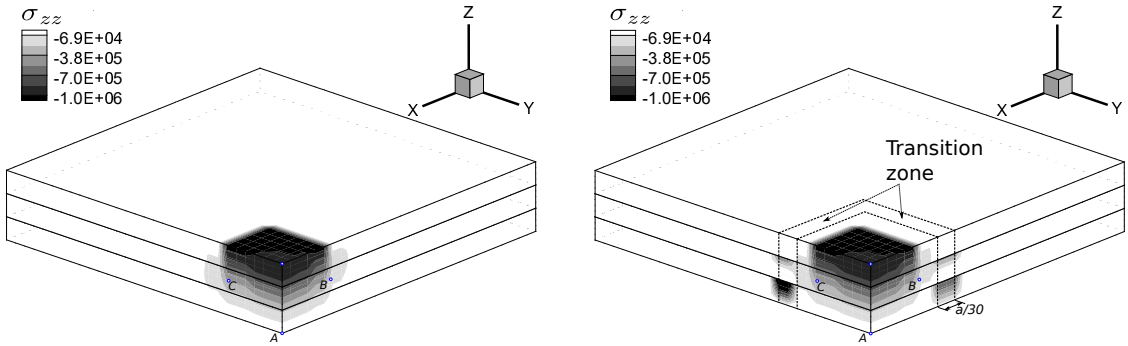

(a) LE5 (b) TE3Z-LE5

Figure 14: Contour plot of σ_{zz} on the three-layered plate under local pressure.

6 Conclusions

Based on Carrera Unified Formulation (CUF), node-dependent kinematics is presented as an innovative approach to constructing advanced elements, which can be applied to build FE models for global-local analysis. Plate elements with node-dependent variable ESL/LW kinematics are developed and implemented in the global-local analysis of laminated structures. Through the numerical investigation, the following conclusions can be drawn:

- Node-dependent kinematics provides a convenient approach to integrating different types of thickness functions into advanced plate elements.
- With such elements, a kinematic variation can be realized in the range of one element, leading to a transition zone bridging a refined local model to a less-refined peripheral one.
- Elements with variable ESL/LW kinematics from node to node can be conveniently implemented.
- By avoiding using any *ad hoc* coupling method, the compactness of the FE formulations can be kept when node-dependent kinematics is applied to build global-local models.
- With node-dependent kinematics, it is convenient to construct a global-local FE model by simply changing the kinematic theories on the desired nodes without any additional operation on the mesh grids.

- Global-local models constructed with node-dependent kinematics integrating ESL/LW capabilities can achieve comparable numerical accuracy with refined LW models at much fewer computational costs.
- As an innovative and versatile approach, node-dependent kinematics can be employed to build numerically efficient FE models for the analysis of multi-layered structures.

7 Acknowledgment

This research work has been carried out within the project FULLCOMP (FULLy analysis, design, manufacturing, and health monitoring of COMPosite structures), funded by the European Union Horizon 2020 Research and Innovation program under the Marie Skłodowska Curie grant agreement No. 642121.

References

[1] W. Koiter, On the foundations of the linear theory of thin elastic shell, Proc Kon Nederl Akad Wetensch 73 (3) (1970) 169–195.

[2] P. Naghdi, The theory of plates and shells, Handbuch der Physik, vol. VI a-2 (1972) 425–640.

[3] E. Carrera, Theories and finite elements for multilayered, anisotropic, composite plates and shells, Archives of Computational Methods in Engineering 9 (2) (2002) 87–140.

[4] E. Carrera, M. Cinefra, G. Li, G. Kulikov, MITC9 shell finite elements with miscellaneous through-the-thickness functions for the analysis of laminated structures, Composite Structures 154 (2016) 360–373.

[5] E. Carrera, M. Cinefra, G. Li, Refined finite element solutions for anisotropic laminated plates, Composite Structures (2017) –doi:http://dx.doi.org/10.1016/j.compstruct.2017.01.014.

[6] M. Cinefra, S. Valvano, E. Carrera, Heat conduction and thermal stress analysis of laminated composites by a variable kinematic MITC9 shell element, Curved and Layered Structures 2 (1).

[7] M. Cinefra, S. Valvano, A variable kinematic doubly-curved MITC9 shell element for the analysis of laminated composites, Mechanics of Advanced Materials and Structures 23 (11) (2016) 1312–1325.

[8] R. E. Bank, The efficient implementation of local mesh refinement algorithms, Adaptive Computational Methods for Partial Differential Equations (1983) 74–81.

[9] B. Szabó, A. Düster, E. Rank, The p-version of the finite element method, Encyclopedia of computational mechanics.

[10] J. N. Reddy, An introduction to the finite element method, Vol. 2, McGraw-Hill New York, 1993.

[11] D. M. Thompson, O. H. Griffin, et al., 2-d to 3-d global/local finite element analysis of cross-ply composite laminates, Journal of Reinforced Plastics and Composites 9 (5) (1990) 492–502.

[12] E. J. Holm, H. Petter Langtangen, A unified mesh refinement method with applications to porous media flow, International Journal for Numerical Methods in Fluids 28 (1998) 679–702.

[13] J. D. Whitcomb, K. Woo, Application of iterative global/local finite-element analysis. part 1: Linear analysis, International Journal for Numerical Methods in Biomedical Engineering 9 (9) (1993) 745–756.

[14] J. Fish, L. Pan, V. Belsky, S. Gomaa, Unstructured multigrid method for shells, International Journal for Numerical Methods in Engineering 39 (7) (1996) 1181–1197.

[15] J. Fish, The s-version of the finite element method, Computers & Structures 43 (3) (1992) 539–547.

[16] J. W. Park, J. W. Hwang, Y. H. Kim, Efficient finite element analysis using mesh superposition technique, Finite Elements in Analysis and Design 39 (7) (2003) 619–638.

[17] J. Reddy, D. Robbins, Theories and computational models for composite laminates, Applied Mechanics Reviews 47 (6) (1994) 147–169.

[18] J. N. Reddy, Mechanics of laminated composite plates and shells: theory and analysis, CRC Press, 2004.

[19] W. Prager, Variational principles of linear elastostatics for discontinuous displacements, strains and stresses, Recent Progress in Applied Mechanics. The Folkey Odquist Volume. Stockholm: Almquist and Wiksell (1967) 463–474.

[20] M. A. Aminpour, J. B. Ransom, S. L. McCleary, A coupled analysis method for structures with independently modelled finite element subdomains, International Journal for Numerical Methods in Engineering 38 (21) (1995) 3695–3718.

[21] J. B. Ransom, On Multifunctional Collaborative Methods in Engineering Science, Tech. rep. (Sep. 2001).

[22] F. Brezzi, L. D. Marini, The three-field formulation for elasticity problems, GAMM-Mitteilungen 28 (2) (2005) 124–153.

[23] P. Blanco, R. Feijóo, S. Urquiza, A variational approach for coupling kinematically incompatible structural models, Computer Methods in Applied Mechanics and Engineering 197 (17) (2008) 1577–1602.

[24] P. Blanco, P. Gervasio, A. Quarteroni, Extended variational formulation for heterogeneous partial differential equations, Computational Methods in Applied Mathematics Comput. Methods Appl. Math. 11 (2) (2011) 141–172.

[25] C. Wenzel, P. Vidal, M. D'Ottavio, O. Polit, Coupling of heterogeneous kinematics and finite element approximations applied to composite beam structures, Composite Structures 116 (2014) 177–192.

[26] E. Carrera, A. Pagani, M. Petrolo, Use of Lagrange multipliers to combine 1D variable kinematic finite elements, Computers & Structures 129 (2013) 194–206.

[27] E. Carrera, A. Pagani, Analysis of reinforced and thin-walled structures by multi-line refined 1d/beam models, International Journal of Mechanical Sciences 75 (2013) 278–287.

[28] E. Carrera, A. Pagani, Multi-line enhanced beam model for the analysis of laminated composite structures, Composites Part B: Engineering 57 (2014) 112–119.

[29] H. B. Dhia, Multiscale mechanical problems: the Arlequin method, Comptes Rendus de l'Academie des Sciences Series IIB Mechanics Physics Astronomy 12 (326) (1998) 899–904.

[30] H. B. Dhia, G. Rateau, The Arlequin method as a flexible engineering design tool, International Journal for Numerical Methods in Engineering 62 (11) (2005) 1442–1462.

[31] F. Biscani, G. Giunta, S. Belouettar, E. Carrera, H. Hu, Variable kinematic beam elements coupled via Arlequin method, Composite Structures 93 (2) (2011) 697–708.

[32] F. Biscani, G. Giunta, S. Belouettar, E. Carrera, H. Hu, Variable kinematic plate elements coupled via arlequin method, International Journal for Numerical Methods in Engineering 91 (12) (2012) 1264–1290.

[33] F. Biscani, P. Nali, S. Belouettar, E. Carrera, Coupling of hierarchical piezoelectric plate finite elements via arlequin method, Journal of Intelligent Material Systems and Structures 23 (7) (2012) 749–764.

[34] Q. He, H. Hu, S. Belouettar, G. Guinta, K. Yu, Y. Liu, F. Biscani, E. Carrera, M. Potier-Ferry, Multi-scale modelling of sandwich structures using hierarchical kinematics, Composite Structures 93 (9) (2011) 2375–2383.

[35] N. Pagano, S. Soni, Global-local laminate variational model, International Journal of Solids and Structures 19 (3) (1983) 207 – 228.

[36] R. Jones, R. Callinan, K. Teh, K. Brown, Analysis of multi-layer laminates using three-dimensional super-elements, International Journal for Numerical Methods in Engineering 20 (3) (1984) 583–587.

[37] M. DOttavio, L. Dozio, R. Vescovini, O. Polit, Bending analysis of composite laminated and sandwich structures using sublaminate variable-kinematic ritz models, Composite Structures 155 (2016) 45–62.

[38] D. Robbins, J. Reddy, Variable kinematic modelling of laminated composite plates, International Journal for Numerical Methods in Engineering 39 (13) (1996) 2283–2317.

[39] E. Carrera, M. Cinefra, M. Petrolo, E. Zappino, Finite element analysis of structures through Unified Formulation, John Wiley & Sons, 2014.

[40] E. Carrera, E. Zappino, Analysis of complex structures coupling variable kinematics one-dimensional models, in: ASME 2014 International Mechanical Engineering Congress and Exposition, American Society of Mechanical Engineers, 2014, pp. V001T01A023–V001T01A023.

[41] E. Carrera, M. Filippi, A. Pagani, E. Zappino, Node-dependent kinematics, refined zig-zag and multi-line beam theories for the analysis of composite structures, in: 58th AIAA/ASCE/AHS/ASC Structures, Structural Dynamics, and Materials Conference, 2017, p. 0425.

[42] E. Carrera, A. Pagani, S. Valvano, Multilayered plate elements accounting for refined theories and node-dependent kinematics, Composites Part B: Engineering (2017) – doi:http://dx.doi.org/10.1016/j.compositesb.2017.01.022.

[43] H. Murakami, Laminated composite plate theory with improved in-plane responses, Journal of Applied Mechanics 53 (3) (1986) 661–666.

[44] M. Cinefra, C. Chinosi, L. Della Croce, MITC9 shell elements based on refined theories for the analysis of isotropic cylindrical structures, Mechanics of Advanced Materials and Structures 20 (2) (2013) 91–100.

[45] K. Surana, S. Nguyen, Two-dimensional curved beam element with higher-order hierarchical transverse approximation for laminated composites, Computers & Structures 36 (3) (1990) 499–511.

[46] X. Lin, Y. Zhang, A novel one-dimensional two-node shear-flexible layered composite beam element, Finite Elements in Analysis and Design 47 (7) (2011) 676 – 682.

[47] J. F. Davalos, Y. Kim, E. J. Barbero, Analysis of laminated beams with a layer-wise constant shear theory, Composite Structures 28 (3) (1994) 241–253.

[48] T. P. Vo, H.-T. Thai, Static behavior of composite beams using various refined shear deformation theories, Composite Structures 94 (8) (2012) 2513–2522.